# A Treatise of the Physical Aspects of Phosphenes and Single-Cell Selectivity in Retinal Stimulation

Research Article

Villarreal DL*, Schroeder D, Krautschneider WH

Institute of Nano- and Medical Electronics, Hamburg University of Technology, Hamburg, Germany.

## Abstract

**Objective:** Artificial vision is currently in an early-stage of maturity. This can be understood as a falling short of visual prosthesis to generate a complete visual scene with detail perception. Similarly, the physical aspects of phosphenes or spots of light demand a better understanding.

**Approach:** This study introduces the strategy of the activation area and pinpoints its usefulness to estimate the amount of cells activated and identify the size and shape of the phosphenes. A simulation framework was built by integrating the relevant retinal interface elements and the dynamics of the ionic channels in the ganglion cells. Shape perceptions reported by Keserü in clinical trials were directly compared with our simulation framework. Similarly, the strategy of the activation area is used on a proposed electrode array to activate single cells and to produce a small spot of light required for high-resolution vision.

**Main Results:** The wide range of shape responses formerly described by patients is highly correlated with our simulation-based findings. Single-cell selectivity was reached throughout the regions near the fovea, which is necessary in humans for activities where visual detail is of primary importance and thus relevant for high resolution vision. For realistic applications, we provided the dimensions of the electrode carrier for single localized stimulation.

**Significance:** Together of being useful to identify the physical aspects of phosphenes generated by electrical stimulation, the applicability of the activation area can yield valuable strategies to attain single-cell selectivity.

**Keywords:** Phosphenes; Pixelized Visual Perception; Prosthetic Vision; Physical Aspects of Phosphenes; Retina Implant; Single-Cell Selectivity; Simulating Visual Prosthet.

## Introduction

PROSTHETIC vision is built upon phosphenes [1]. A phosphene is defined as any visual sensation represented as a spot of light in the visual field caused by methods other than stimulation of the visual system by light. Phosphenes can be elicited by mechanical forces [2], magnetic stimulation [3-5] or electrical stimulation [6-15].

In recent years, epi-and subretinal implants have been developed [6-15]. Humayun et al., [6-9], Mahadevappa et al., [10], Rizzo III et al., [11, 12], Klauke et al., [13], Eger et al., [14] and Keserüet al., [15] and recent clinical trials [16, 17] have reported that blind patients perceived sensations of spots of light while the retina was electrically stimulated. These experiments clearly validated the viability of producing perception of light patterns in blind patients by electrically activating nearby retinal ganglion cells (RGCs). In recent years, Humayun et al., [7, 9], Keserü et al., [15], Dobelle et al., [18, 19], Zrenner et al., [20, 21], Brindley et al., [22, 23] and Hornig et al., [24] have reported the generation of recognizable symbols and simpleshapes from multiple stimulated phosphenes.

Phosphenes have been observed in the form of doughnut shapes [8], punctuate spots of light when occurring close to the center of the visual field [18, 19], elongated shapes [22, 25], lines/bars [25, 26], triangles [26], and more complicated patterns [26]. Phosphenes are commonly described as "round" spots of light [8-10, 15, 25, 27] and carrying some colors, such as red [26], blue

**\*Corresponding Author**:
Diego Lujan Villarreal,
Institute of Nano- and Medical Electronics, Hamburg University of Technology, Hamburg, 21073, Germany.
Tel: +49 40 42878 3991
Fax: +49 40 42878 2877
E-mail: diego.lujan@tuhh.de

Villarreal DL, Schroeder D, Krautschneider WH. A Treatise of the Physical Aspects of Phosphenes and Single-Cell Selectivity in Retinal Stimulation. *Int J Comput Neural Eng.* 2017;4(2):55-70.

55

[8, 23, 26], yellow [8, 23, 26], orange [8, 18, 26] and multicolor [26].

Visual prostheses would ideally reproduce accurately natural spatiotemporal patterns of activity in the RGCs. This requires the capacity of each electrode to reach single-cell selectively. In other words, RGCs are tightly-packed in the ganglionic layer, mainly at the fovea. Unique characteristics of the visual space are sent to the brain by temporal patterns of activity in RGC types that are spatially mixed. Hence, RGCs that are close to each other frequently transmit very different signals [28].

For as much as phosphenes are the single elementary building block in prosthetic vision, investigators have sought to create richer and more complex patterns to represent visual scenes while the retina is electrically stimulated. The foremost concern is that advanced retinal implants induce atypical patterns of retinal activity [16, 17]. Relatively large electrode diameter in implanted devices [10, 12, 14, 16, 17] likely activates hundreds or thousands of cells over their area of stimulation. Not only does this coarse stimulation of cells restrict detailed perception, but also the activity generated by stimulation remains dissimilar to the healthy retina [29].

Current clinical trials demonstrate that patients do not obtain a complete visual scene composed of simultaneously presented phosphenes. Recent clinical trials associated with Argus II developed by Second Sight Medical Products in the United States exhibited a best measured visual acuity of 20/1260 in 7 out of 30 test volunteers [16]. Similar conclusions have lately been reached by Alpha IMS developed by Retina Implant AG in Germany that reported a best visual acuity of 20/546 in 2 out of 9 test volunteers [17].

Current strategies for single-cell selectivity have proven to be inadequate [16, 17]. To evoke a narrow spot of light that resembles a natural signal to the brain and can serve as a building block for the pattern of phosphenes, each electrode should activate a nearby cell [30].

As artificial vision is currently in an early-stage of maturity, the physical basis of phosphenes in prosthetic vision demands a better understanding. Together with a grasp of attaining single-cell selectivity would be then a requirement to align retinal stimulation with a high-stage of maturity.

This paper introduces the activation area and pinpoints its usefulness to estimate the amount of cells activated and to identify the size and shape of the phosphenes. To prove the activation area, our results were directly compared with the shape perceptions reported by Keserü in clinical trials. Later, the strategy of the activation area is used on a proposed electrode array to activate single cells and to produce a small spot of light required for high-resolution vision.

This paper is organized in two main sections. Section II is devoted to prove the activation area. Section III is dedicated to introduce a new method for achieving single cell stimulation per stimulating electrode. Each section is subdivided in materials and methods, results and discussion.
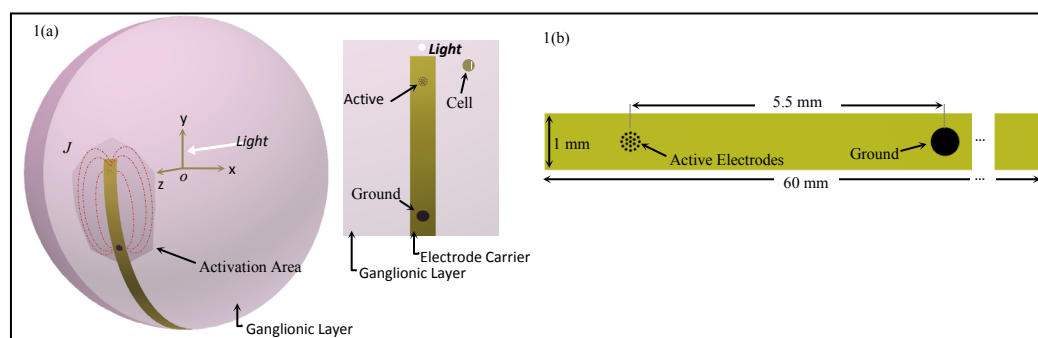
## Proof Of Activation Area

### Materials and Methods

***Definition and Procedure of the Activation Area:*** The activation area is defined as a space on the retina where the stimulus initiated at the active electrode in effect triggers a response of some cells. The activation area can estimate the amount of cells activated and identify the size and shape of the phosphenes. The criterion of the activation area states that a cell located inside the activation area is activated by the respective electrode. Otherwise, the cell is not activated by this electrode.

Figure 1(a) shows an example of the activation area related to the flexible film electrode carrier developed by Keserü et al., [15]. In this example, an array of active electrodes injects charge density to trigger a response of some ganglion cells.

The shape of the activation area is related to the spreading direction of current density from the active electrodes to ground. The broadness of the activation area has a close relationship with the amount of peak current injected to the electrode. The current density spreads throughout the medium that consists of layers of tissue. At the location of the electrodes, the intensity of the current density has the highest degree. As the distance to the electrodes increases, the current density becomes insufficient to trigger a response of the cell and the activation area is brought to an end. Thus, phosphenes generated by artificial stimulation can be associated with the activation area. In this regard, section III-D

**Figure 1. (a) Activation area related to the flexible film electrode carrier shown in figure 1(b) by applying a charge density. The shape of the activation area is associated with the spread of current density, *J*, throughout the medium to the electrode ground. The broadness is related to the amount of peak charge injected. 1(b) Electrode carrier with an effective electrode diameter of 50, 200 and 360 μm.**

lists the supporting evidence.

The simulation algorithm of the activation area is as shown in figure 2. The algorithm is designed as to meet two paths, 1) phosphene shape description based on a predefined current injection and 2) controlled-shape phosphene based on a specific current injection. This multidirectional algorithm can ensure the activation of cells within determined safety limits.

The inputs in the algorithm are stimulating parameters (i.e. injected current i, pulse duration, pulse shape and domain properties) and geometric parameters (i.e. cell location $C$, domain dimensions, proximity of cell to electrode and electrode distribution).

The first path of the algorithm can identify the size and shape of the phosphene. This path is shown in figure 2. Fixed inputs during the implementation are all the geometric and stimulation parameters except the location of the cell. The variability of cell location is explained in the corresponding section. This path is executed until enough boundary points are recorded to enclose the area of activation (not shown in figure 2. For more information, see step f). For the proper operation of the algorithm, the initial values of cell location, $C=(x_e, y_e, z_e)$ should be such that the cell is placed inside the ganglionic layer, exactly below the center of active electrode and enclosed with the cell membrane.

The second path of the algorithm is created to restrict the spread of the stimulus to the space required for activation. This path is shown in figure 2. Fixed inputs are all the geometric and stimulation parameters except the injected current. The variability is explained as follows. The cell can bemoved to a desired distance inside the ganglionic layer, see figure 3b. This path is executed until the threshold injected current across the electrodes is found. This threshold current will restrict the current spread across the electrodes and the region of stimulation will be controlled by this specific current injection. Afterwards, input

stimulation parameters take this threshold as the injected current, $i$, and the activation area is generated based on the first path of the algorithm. As a reminder, the location of the cell becomes a variable parameter.
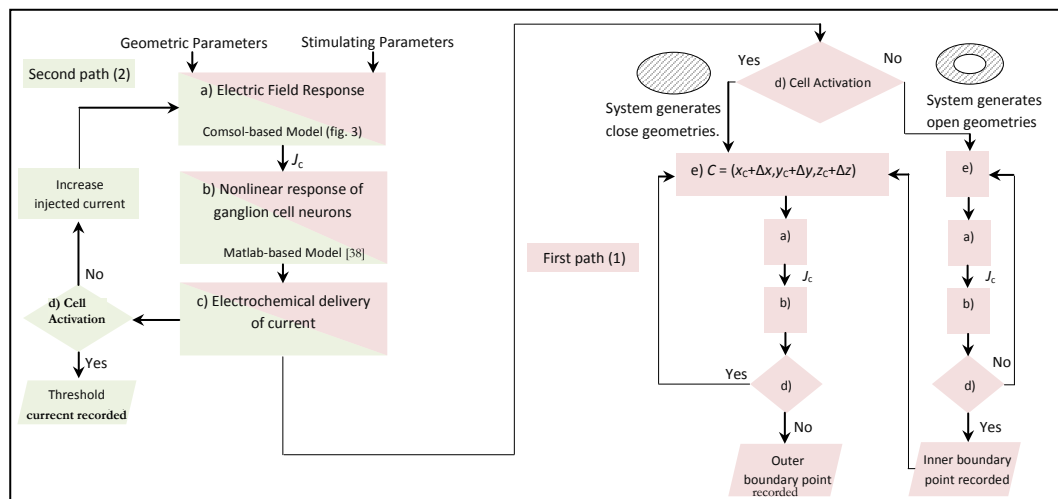
Each processing step is further explained in sequential order based on its appearance.

**Electric Field Response:** A 3D computational model of electrical stimulation was implemented in COMSOL Multiphysics software (COMSOL, AB., Sweden, Version 4.4), see figure 3. The model similar to [31] consists of one half of a sphere that represents a segment of the human eye. The inner surface of the retina has a diameter of 22 mm. Experimental data of microelectrodes coated with PEDOT-NaPSS was used in our model. PEDOT-NaPSS was applied by electrode position with a charge density of 40 mC/cm². This results in a thin thickness of 200 nm [32]. The layers included in the simulation model are the polyimide carrier of the electrodes, vitreous medium, photoreceptor layer, ganglionic layer, ganglion cell soma and retinal pigment epithelium. The ganglion cell soma was placed inside the ganglionic layer. This schematic representation of the retina is built to a greater degree of anatomical likeness than previously published works [33]. The retinal network models (i.e. bipolar, horizontal and amacrine cells, ON- and OFF networks) are excluded because of severe rod and cone photoreceptor impairment that cannot drive synaptic connection started with a photocurrent input. The proper conductivity, permittivity and thickness of the layers formerly mentioned can be found in table I [34-37].

The 3D model operates with an array of electrodes as shown in figure 1(b). Biphasic pulses of uniform current are injected from the active to ground electrodes to drive stimulation of nearby cells. We extracted from Comsol the peak boundary current density in the membrane that encloses the ganglion cell. Other extracted

**Figure 2. The algorithm of the activation area. The first and second paths are enclosed with red and green geometrical shapes, respectively. Geometric and stimulation parameters serve as inputs during the operation. Nonlinear response of the cell uses the peak boundary current density in the membrane ($J_c$) from Comsol simulation as an input in the circuit model. The algorithm supports electrochemical safety to ensure safe stimulus delivery and cell activation. The cell is initially placed exactly below the center of active electrode and enclosed with the cell membrane. In the first path, cell location, $C$, is incremented by $\Delta x$, $\Delta y$, $\Delta z$ in each iteration. The algorithm is implemented until the area of activation becomes an enclosed-based percept (see step f). Steps showing single letters are related to the corresponding actions in the algorithm.**



Villarreal DL, Schroeder D, Krautschneider WH. A Treatise of the Physical Aspects of Phosphenes and Single-Cell Selectivity in Retinal Stimulation. *Int J Comput Neural Eng.* 2017;4(2):55-70.

data are the voltage across the electrodes and current delivered by the electrode.

**Nonlinear Response of Cell Neurons:** We assumed that the peak boundary current density in the cell membrane serves as an input parameter in the circuit model of the RGC. The RGC circuit model was developed by Fohlmeister et al., [38]. The basic mathematical structure for voltage-gated ion channels was based on the Hodgkin and Huxley like equations [39]. This modelling assumption was formulated in Joucla S, et al., (2014) [40] where the original mathematical model of Hodgkin and Huxley was used. The parameters and equations that describe the dynamics of the ionic channels were kept as in the original model [38].

This externally applied current density is distributed to the participating channel types found in this particular cell membrane. The threshold injected current required for the activation of a cell by means of extracellular stimulation must generate a voltage shift of around +30 mV in the cell membrane. The extracellular current density across the cell membrane computed in Comsol simulation is assumed to be equal to the circuit modelling of ganglion cell. Hodgkin and Huxley-like equations can describe the eliciting of action potential in the cell membrane.

A Matlab (MathWorks, Inc., United States, Version 7.13) script implemented the ganglion cell circuit model and determined the stimulation of the RGC. LiveLink for Matlab was used to integrate the 3D computational model built in Comsol Multiphysics to the Matlab scripting environment.

**Electrochemical Safety:** Electrochemical safety must guarantee that the voltage across the electrodes, local charge density on the electrode and the heat generated by the device must be within the safe electrochemical limits. As such, electrolysis of water, the formation of corrosion [41] and excessive tissue heating that leads to significant damage to various cellular functions [42] must be avoided. A Matlab script organized the extracted data of voltage across the electrodes and current delivered by the electrode and performed several tasks to obtain the heat dissipated at the device and charge density on the electrode.

Local charge density was obtained by integrating the current delivered by the active electrode over time and dividing it by the electrode area. Neural tissue heating from the retina implant is calculated using a linear approach of $\Delta T = 1°C$ per 12.2 mW/cm$^2$ [42] assuming only heat conduction. Body temperature of 37° degrees was the initial value. A temperature limit of 1°C was assumed [44]. The power density at the device was obtained by following the approach seen in Luján Villarreal D, et al., (2016) [31] of 1024 evenly distributed electrodes, each with low power consumption of 54 μW [45] of an existing stimulator device.
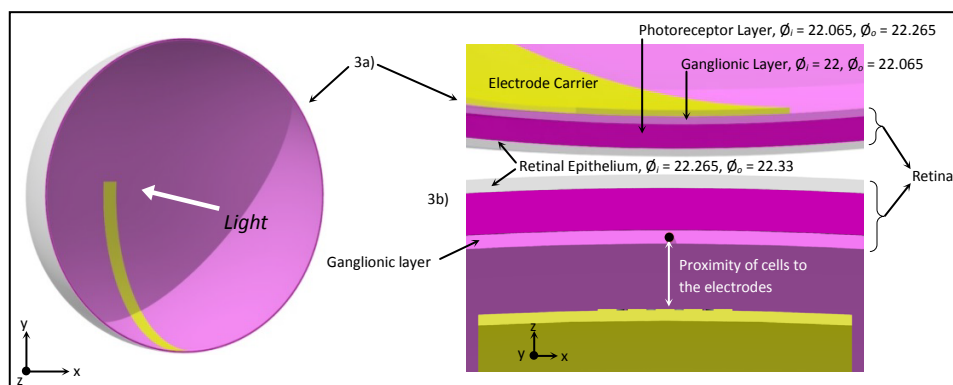
PEDOT voltage window extends beyond conductive materials, such as MnO$_2$, from 1.5V up to 1.7V [43]. Since the values of the

**Table 1. Description Of The Values Of Simulation.**

| Layer | Conductivity [S/m] | Permittivity [-] | Thickness [μm] |
|---|---|---|---|
| Polyimide Carrier | 1e-17 | 1 | 65[1] |
| Vitreous Humor | 1.5 | 98 | 22e3[2] |
| Epithelium Layer | 2e-3 | 1 | 65[1] |
| Photoreceptor Layer | 28.5e-3 | 1 | 200 |
| Intracellular space | 10e-3 | 3.98e-11 | 30 |
| PEDOT-NaPSS coating | 400 | 1 | 0.2 |
| Contact conductivity[3] | 321 | - | - |
| Cell membrane | 1e-8 | 8.8e-11 | 0.01[4] |
| Ganglionic Layer | 10e-3 | 1 | 65[1] |

[1] Comsol minimum thickness of surface sphere is 65 μm. [2] Value of vitreous humor is its diameter. [3] Conductivity is of the contact of PEDOT-NaPSS deposition and tissue. [4] Value is the thickness of cell membrane.

**Figure 3. a) Simulation model built in Comsol Multiphysics. Ø$_i$ and Ø$_o$ are defined as inner and outer surface diameter (given in units of mm). Complete information of each model is listed in table I; 3b) shows the proximity of cells to the electrodes and the ganglionic layer where the cell can be moved.**



Villarreal DL, Schroeder D, Krautschneider WH. A Treatise of the Physical Aspects of Phosphenes and Single-Cell Selectivity in Retinal Stimulation. *Int J Comput Neural Eng.* 2017;4(2):55-70.

voltage window of low-area electrodes were not published [32], an average limit of 1.7V is assumed. The charge density limit of 1 mC/cm² is assumed considering that the values of safe charge density of low-area electrodes coated with PEDOT-NaPSS were not published [32].

**Cell Activation:** The threshold current necessary for cell activation in the form of extracellular stimulation must produce depolarization in the cell membrane. The circuit modelling of the RGC in the tiger salamander developed by Fohlmeister et al., [38] is sufficient to describe the cell depolarization in response to various levels of extracellular stimulation [40]. Hence, the amplitude of the injected current from the active electrode must be large enough to attain the formerly stated task.

**Cell Location:** As previously stated, the cell is initially placed inside the retina ganglion cell layer and exactly below the center of active electrode.

If the extracellular current density is large enough to trigger a response (Yes-decision) a percept where the surface forms a closed geometry is generated. Then, the cell is shifted inside the ganglionic layer (see figure 3b) until the outer boundary of activation is found. Next, this boundary point can be recorded.

Once the extracellular current density is not large enough for stimulation (No-decision), two possibilities can occur; i) a percept where the surface forms an opened geometry is created, e.g. ring-shaped percept, or ii) there is no such thing as electrical stimulation.

For the former case, the cell is shifted inside the ganglionic layer until the inner boundary of activation is found. Then, this boundary point surrounding the active electrode can be recorded. For the latter case, if the cell has been shifted without having stimulation, an increase of the injected current must be performed.

**Enclosed Area Generation (not shown in Figure 2):** The algorithm is implemented until the area of activation becomes an enclosed-based percept. If the area of activation is not an enclosed geometry, the cell location returns to its initial value of being exactly below the center of active electrode (return to step e) and the cell is shifted but in another direction. Since the number of points to enclose a region can be as finite as the desire of the user, a recommendation would be to enclose the percept using an octagonal-based framing.

Once the activation area is generated, the criterion asserts that a cell located inside the activation area is activated by the respective electrode. Otherwise, the cell is not stimulated by this electrode.

**Calculation of RGC Activation:** Consider an arbitrary activation area which is divided into regular shapes that together form a region that is similar to the activation area. The total number of ganglion cells activated is calculated as the sum of the areas of these individual regular shapes multiplied by a local ganglion cell density.

$$G = \sum_{j=1}^{n} \Delta A_j \cdot \rho_{Cj} \qquad ----(1)$$

$G$ is the cells stimulated, $\Delta A$ is the area of the individual regular shapes, $j$ is a subinterval and $\rho_C$ is the area cell density. Watson [46] gave an equation to obtain the ganglion cell density found by Curcio [47] as a function of the eccentricity.

$$\rho_C(r',k) = \rho_C(0) \times \left[ a_k \left( 1 + \frac{r'}{r_{2,k}} \right)^{-2} + (1 - a_k) \exp\left( -\frac{r'}{r_{e,k}} \right) \right] ----(2)$$

$\rho_c(0)$ is the peak ganglion cell density of 33162 in units of deg$^{-2}$, $a_k$ is the weighting of the first term, $r'$ is eccentricity in units of degrees, $r_{2,k}$ and $r_{e,k}$ are scale factors. The meridian is indicated by the index $k$. The estimated parameters for each meridian as well as unit conversion equations from degrees to millimeters can be found in Watson AB (2014) [46].

We generated a computational-based map of ganglion cell using the cell density equation (1) and the assumption that within any one quadrant of the retina the iso-spacing contours are elliptical-based forms. This idea leads to an equation to obtain the ganglion cell density at an arbitrary point $\{x,y\}$ on the retina [46].

$$\rho_C(x,y) = \frac{r_{xy}^2 \rho_C(r_{xy},1) \rho_C(r_{xy},2)}{x^2 \rho_C(r_{xy},2) + y^2 \rho_C(r_{xy},1)} ----- (3)$$

$r_{xy}$ is the radial eccentricity of the point $\{x, y\}$ obtained as $(x^2 + y^2)^{0.5}$, 1 and 2 in eq. (3) represent the vertical and horizontal meridians, respectively.

**Clinical Trial Results for Comparison:** A clinical trial was carried out to test an electrode carrier that was implanted in 20 volunteers with different stages of retinitis pigmentosa (RP), rod-cone dystrophy or usher syndrome retinal degeneration [15]. The objectives of the study were to measure the perception threshold and to identify the shape of the phosphenes induced by electrical stimulation.

The electrode carrier consists of a flexible film of around 10 μm thick, 1 mm wide and 60 mm long. The electrode carrier followed a ring-electrode approach with effective electrode diameter of 50, 200 and 360 μm. The ground electrode has a diameter of 560 μm and is placed 5.5 mm away from the stimulation electrodes, see fig. 1(b) or 4(a).

The perceptual threshold was measured in 15 patients using an effective electrode diameter of 360 μm, see figure 4(a), and selecting either a single, see figure 4(b), or multiple electrode stimulation, see figure 4(c).

The results revealed a wide range of perceptual thresholds ranging from 20 to 768 nC (i.e. from 0.02 to 0.75 mC/cm²) for both single and multiple electrode stimulation. The patients were asked to describe the perceived objects in their own words. Although a single electrode was active, a wide range of shapes were revealed, such as a circle, ring, rectangle, hash mark, half paperclip, '@' sign, fan-like arrangement, etc.

Due to the time slot between stimulation and postoperative interviews, the patients were not able to assign the perceptual

Villarreal DL, Schroeder D, Krautschneider WH. A Treatise of the Physical Aspects of Phosphenes and Single-Cell Selectivity in Retinal Stimulation. *Int J Comput Neural Eng.* 2017;4(2):55-70.

59

**Figure 4. Three different electrode arrays. 4(a) Electrode array of 50, 200 and 360 effective diameters [15]. 4(b) Single electrode stimulation. 4(c) Multiple electrode stimulation. The electrodes are in contact with the retinal surface layer. 4(d) Position of the electrode carrier inside the eye.**
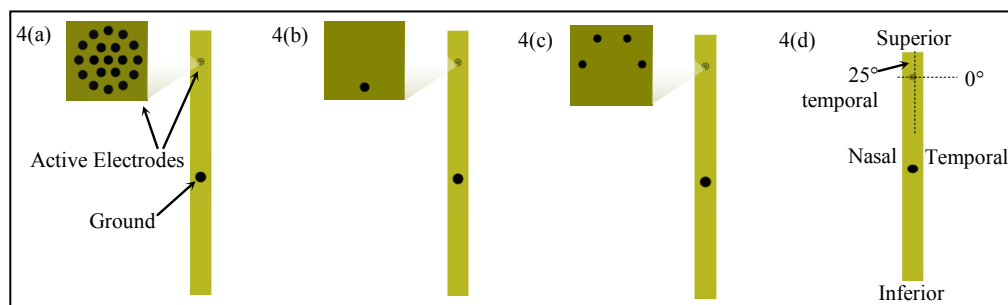


shapes to individual stimulation sequences. For more information about threshold response verification see [15].

***Verification of FEM-based Simulation Model:*** Keserü and colleagues coated the electrodes with IrOx. IrOx allows considerably greater levels of charge injection without electrode dissolution or electrolysis of water.

IrOx has been used to coat a variety of electrodes including deep brain, nerve cuff, pacing, and defibrillation electrodes [49-51]. Despite that the specifics of IrOx deposition and contact conductivity with tissue were not published in Keserü M, et al., (2012) [15], there is evidence that carbon nanotube-polyelectrolyte electrodes coated with IrOx at 160 mC/cm² charge density deposition [52] have similar impedance characteristics to PEDOT-NaPSS nanotubes [32] up to 10 kHz.

However, the thicknesses and impedances of coating materials such as IrOx [52] and PEDOT-NaPSS [32] are influenced by the charge density deposition. Likewise, the technique of deposition, layer thickness, chemical composition and micro/nanoscale morphology and topography have a considerable influence on the electrical, mechanical and biological interfacing properties of the electrodes [52].

Keserü measured the mean voltage amplitude of 1.82 V for single electrode stimulation and a charge of 380 nC. Using this value as a basis of comparison, a prior verification of the model was performed using Comsol Multiphysics.

PEDOT-NaPSS contact conductivity with tissue calculated in Luján Villarreal D, et al., (2016) [31] was used. The definition of the domains is listed in table I. The contact conductivity listed in that table is related to the interaction of charge transfer with the tissues.

Since the specifics of the exact electrode were not published in Keserü M, et al., (2015) [15], we used a single electrode shown in figure 4(b). The stimulation parameters of pulse shape and duration were kept as in the original experiment, i.e. rectangular biphasic, anodic first of 2 ms of pulse duration followed by cathodic of 1 ms of pulse duration.

The outcome of our simulation model revealed a good agreement with the experimental findings by reaching a value of 1.784 V with 2% of error. Accordingly, PEDOT-NaPSS conductivity with tissue and the definitions of the domains formerly stated can

deliver accurate results of the electric field distribution throughout the retinal tissue.

***Stimulation Parameters:*** In this first section, the experimental findings of perceptual thresholds and the shape of the phosphenes found by Keserü were used to prove the activation area.

To achieve such challenge, the activation area was mapped by following the first path of the simulation algorithm shown in figure 2. Keserü developed a stimulator device that ensures high-standard of safety for applications related to visual shown in figure 4(d).

The stimulation parameters of pulse shape and duration were kept as in the original experiment. Charge-imbalanced rectangular pulse shape is delivered with anodic first with pulse duration of 2 ms followed by cathodic with pulse duration of 1 ms. In-between anodic and cathodic pulse the system is open-circuited with a delay of 100 µs.

Charge densities of 0.02, 0.1, 0.35 and 0.75 mC/cm² were applied across single or multiple electrode configurations. The charge capacity of an electrode material is calculated as the maximum amount of charge per unit area that can be passed in a biphasic pulse without causing eventual electrode damage [15]. Therefore, the peak injected current applied across the electrodes was calculated as:

$$i = \frac{\sigma_q \cdot A_E}{t} \quad \text{---- (4)}$$

$\sigma_q$ is the charge density applied, $A_E$ is the electrode cross section area and t is the total pulse duration of a biphasic pulse shape.

As previously stated, the range of perceptual threshold measured in 15 patients was 20 to 768 nC [15]. The standard deviation was 229.55 nC. This high variability of standard deviation may be related to the distance between the retina surface and the electrode array in different patients in the study [15]. Therefore, the distance between the surface of the retina and the electrode array tested was 10 and 1300 µm.

## Results

Graphical representations of the outer surface dimensions of the activation area are depicted in Figure 5(a) labeled as 'a' to 'd'. Figure 5(b) shows the inner surface dimensions labeled as 'e' to

Villarreal DL, Schroeder D, Krautschneider WH. A Treatise of the Physical Aspects of Phosphenes and Single-Cell Selectivity in Retinal Stimulation. *Int J Comput Neural Eng.* 2017;4(2):55-70.

60

**Figure 5. (a) Graphic representation of the outer surface distances of the activation area labeled as 'a' to 'd'. 5(b) Shows the inner surface distances labeled as 'e' to 'g'. The distances shown in figure 5(b) are relevant when the activation area is a non-closed geometry. 5(c) $\theta_v$ represents the vertical visual angle. 5(d) $\theta_h$ stands for the horizontal visual angle. n stands for the distance from the eye's nodal points to the retina. a and d are some of the dimensions of the activation area, see figure 5(a).**
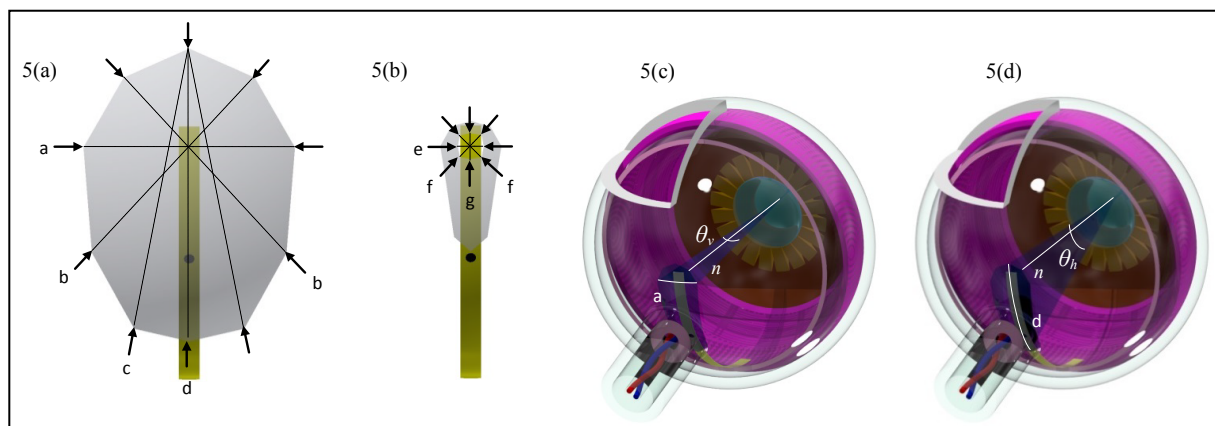


'g'. The dimensions shown in figure 5(b) are relevant when the activation area is a non-closed form. Figure 5(c) shows the vertical visual angle labeled as $\theta_v$ and figure 5(d) shows the horizontal visual angle $\theta_h$. In both figures $n$ stands for the distance from the eye's nodal points to the retina, a and d are some of the dimensions of the activation area, see figure 5(a). Horizontal and vertical visual angles are calculated as:

$$\theta_h, \theta_v = 180\frac{x}{n\pi} \quad ----(5)$$

$x$ is the size of 'd' of the activation area for horizontal visual angle and 'a' for vertical visual angle. The space from the eye's nodal points to the retina is 17 mm [53].

The correlation between the experimental results of Keserü and the activation areas are shown in figure 6 for several charge densities applied across single and multiple electrode stimulation. The x axis shows the charge densities of 0.02, 0.1, 0.35 and 0.75mC/cm², whereas the y axis shows the proximity of cells to the electrode array of 10 and 1300 μm.

As formerly described, the activation area can estimate the shape of the phosphenes. Keserü reported a wide range of shapes with different characteristics, such as a circle, ring, rectangle, hash mark, etc. The outcomes of our simulation framework resulted in a spectrum of elliptical-shapes, either being closed-surface geometries or non-closed.

The shape of an ellipse is denoted by its eccentricity, which is a measure of how much the conic section deviates from being circular. For an ellipse the eccentricity is between 0 and 1. When the eccentricity tends toward 1, the ellipse gets a more elongated shape and can be related to a hash mark or a rectangle. Phosphenes in the form of elongated shapes [22, 25] and lines or bars [25, 26] have also been observed.

When the eccentricity moves away from 1, an ellipse can be related to a circle. Phosphenes were frequently described as "round" spot of lights in Humayun MS (2003), Humayun MS (2004), Mahadevappa M (2005), Keserü M (2011), Rizzo JF (2003), Weiland JD (2004) [8-10, 15, 25, 27]. Once the minor axis

of the ellipse is approximated to the value of 'a' of the activation area, the eccentricity can be calculated as:

$$\varepsilon = \frac{\sqrt{d^2 - a^2}}{d} \quad ---- (6)$$

'd' of the activation area is related to the major axis of an ellipse. Therefore, the shape of the phosphenes recorded by Keserü can be categorized as an elliptical-shaped hash mark (or rectangle) or an elliptical-shaped circle based on their eccentricities.

Despite the fact that most phosphenes were described or otherwise implied as "round" [8-10, 15, 25, 27], it is doubtful that the patients had always defined the shape of the phosphene as a "perfectly circular-shaped phosphene". Such description can include any shape with a smooth, curved circumference, including balls, ovals, and pebbles [1].

Having stated the above, the criterion to identify the shape of phosphenes is as follows. Ring-shaped phosphenes are related to non-closed forms. Hash mark-or rectangular-shaped phosphenes are associated when the eccentricity is higher than 9/10. Circular-shaped phosphenes are related when the eccentricity is lower than 9/10.

The information for each activation area is given in figure 6. The amount of cells activated is computed using eq. (1), where each activation area was divided into 106 regular square regions. Horizontal and vertical visual angles are calculated with eq. 5.

**Discussion**

**Activation Area:** In this study, the activation area is conclusively proven by directly comparing the shape perceptions reported by Keserü and our simulation framework.

Our results exhibited a spectrum of elliptical-shape forms which can be related with circular, hash mark, rectangular or ring-shaped phosphenes.

Villarreal DL, Schroeder D, Krautschneider WH. A Treatise of the Physical Aspects of Phosphenes and Single-Cell Selectivity in Retinal Stimulation. *Int J Comput Neural Eng.* 2017;4(2):55-70.

61

**Circular-Shaped Phosphene:** This specific shaped phosphene belongs to an activation area with an eccentricity lower than 9/10. In essence, figures 6.1 to 6.6 are suitable to this criterion.

Chen et al., stressed that phosphenes should be preferably round [1] because ideally electrodes are required to produce a visual perception of an $m \times n$ array of narrow spots of light that can be precisely controlled by the system.

The previous challenge is associated with single-cell selectivity. Visual perception must be related to the control of each electrode in an array to activate its corresponding cell and elicit a narrow phosphene. Accordingly, one-to-one cell-electrode stimulation can generate a better perception with high-resolution.
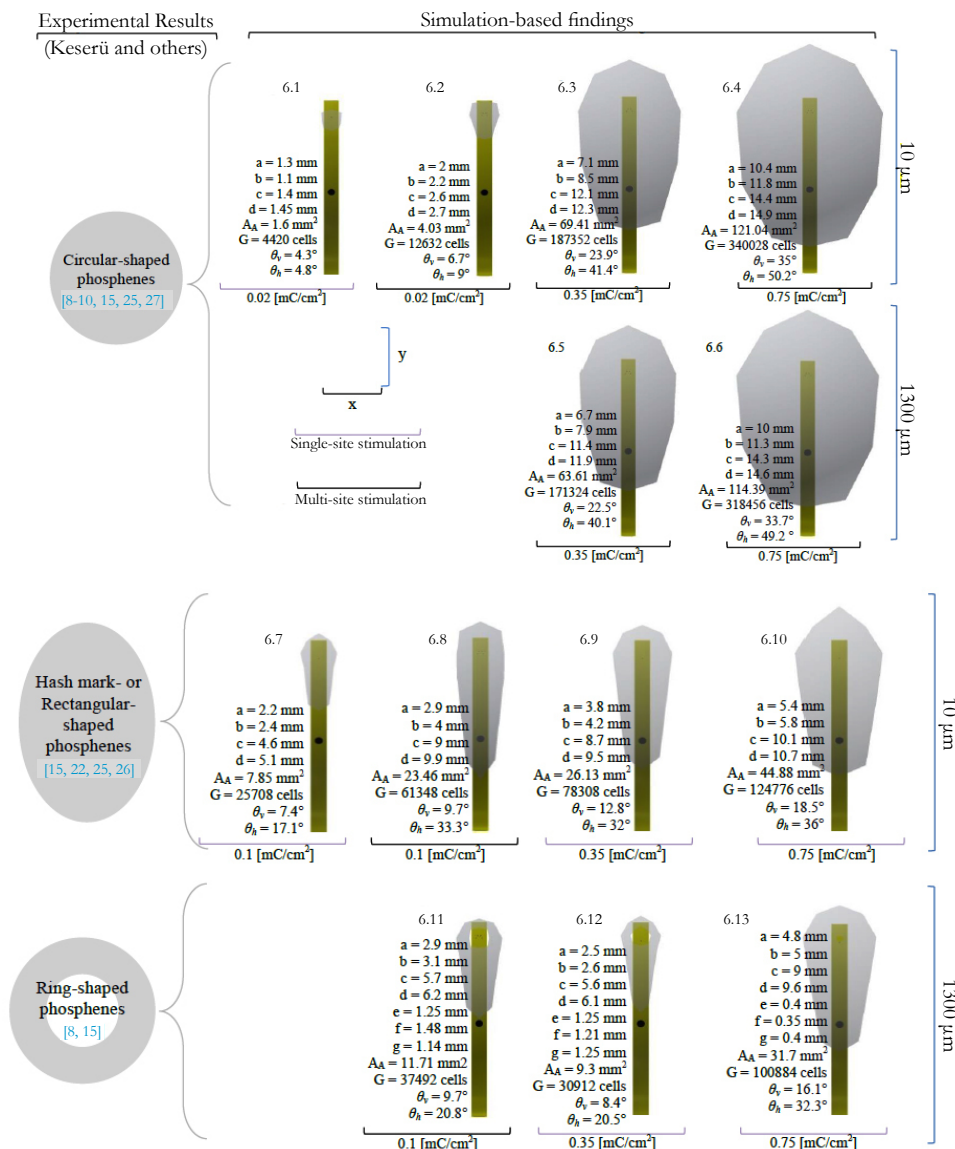
**Hash mark- or Rectangular - Shaped Phosphene:** These particular shaped phosphenes belong to an activation area with an eccentricity higher than 9/10. As such, figures 6.7 to 6.10 are

appropriate to this criterion. Hash mark- or rectangular-shaped phosphenes can be attributed tothe distant location of the ground to the active electrode and to single-electrode configuration. The current spreads deep into the tissues leading to the activation of cells in its path to the ground electrode.

These specific-shaped phosphenes can also be generated by the activation of ganglion cell axons [30]. Retinal ganglion cell axons pass within short distances from each other along their path to the brain. In practice, though, while subjects receive single electrode stimulus, they often report a stripe-shaped phosphene, rather than a focal spot of light due to unintended stimulation of passing axons [54]. This makes difficult to distinguish faces and objects [30].

**Ring-Shaped Visual Phosphene:** Ring-shaped phosphenes belong to an activation area where the surface forms a non-closed geometry. As such, figures 6.11 to 6.13 are suitable for this

**Figure 6. Correlation between simulation-based findings and experimental results. The simulation findings are represented as the activation areas for single and multiple electrode stimulation. X-axis is related to the charge densities applied by the electrodes. Y-axis is associated to the proximity of the cells to the electrodes. In the lower left corner of each activation area is depicted the sizes from 'a' to 'd' for the outer surface dimensions and from 'e' to 'g' for the inner surface dimensions. An empty space inside the plot represents a case where the electrodes could not activate a cell. $A_A$, G, $\theta_h$ and $\theta_v$ are the activation area, number of ganglion cells activated, and horizontal and vertical visual angles, respectively. We assumed to place the electrode array as shown in figure 4(d).**

Villarreal DL, Schroeder D, Krautschneider WH. A Treatise of the Physical Aspects of Phosphenes and Single-Cell Selectivity in Retinal Stimulation. *Int J Comput Neural Eng.* 2017;4(2):55-70.

criterion. Looking carefully, ring-shaped responses arise when the electrode array is in distant proximity to the ganglion cell bodies. Non-closed geometries such as doughnut-shapes have been reported by the patients [8].

When the stimulating electrode is in close proximity to the retinal surface, body cells can be activated with low stimulus amplitudes. This generates small regions of stimulation at the retina. As the proximity increases, the stimulus amplitude needs to be increased to activate some body cells. This contributes to the varying current spread to the ground electrode and causes changes in the area of stimulation.

The closeness is critical not only for the generation of small phosphenes but also for safety limits in stimulation. The major limitation can be attributed to the charge density required to elicit activity in neurons [31]. With close proximity, the threshold current and thus the charge density are reduced, leading to a safe stimulus delivery. Further, the current can be contained in a small volume that surrounds the electrode, leading to a small region of stimulation and possibly the activation of a single cell. Power consumption and thus heat generated by the device [42] are minimized allowing small electrodes to generate phosphenes within safe heat limits [29].

**Perceptual Threshold:** We found that the charge densities and the proximities of the electrodes to the retina generated stimulation of nearby cell bodies see figure. 6. These outcomes were related to the spectrum of perceptual thresholds between 0.02 to 0.75 mC/cm² found by Keserü and colleagues.

**Physical Aspects of Phosphenes:** Our simulation framework having as a basis the activation area proposes the following insights to explain how the shapes of the phosphenes are generated by stimulation.

a) Electrode array topology and characteristics of electrodes influence the shape and breadth of phosphenes. The activation area of single and multiple topologies of stimulating electrodes revealed different shapes of phosphenes e.g. hash mark-shaped percepts and circular-shaped forms. The viable justification of such forms is the far placement of the ground to the active electrode, causing the current to flow deep down into the tissues and activating cells in its path to ground.

Experimental findings which were performed with different experimental setups of electrode topology revealed dissimilar shapes of phosphenes e.g. elongated shapes [22, 25], lines/bars [25, 26, 55], triangles [26], doughnut-shaped [8], complicated patterns [26] and round spots of light [8-10, 15, 25, 27].

b) Cell density in the degenerate retina influences the shape and formation of phosphenes. The variability of thresholds in the experimental findings by Keserü was attributed to a combination of a varying degree of retinal degeneration [15]. This degree of retinal degeneration can influence the shape of the visual perception because gaps of dark vicinities would be exhibited at locations of cell depletion.

c) Single and multiple electrode configurations play a role in the shape and broadness of phosphenes. Our simulation framework revealed that single and multiple electrode stimulation generated different shapes of phosphenes, see figure 6. Experimental observations on the human volunteers by Rizzo et al., [25] and Wilke et al., [55] yielded validating evidence on different shapes of phosphenes such as spots of light or lines by driving one or a line of four electrodes, respectively.

d) The closeness of the cells to the electrodes influences the outline and extent of the phosphenes. With close proximity, body cells can be activated with low stimulus amplitudes. This generates small regions of stimulation at the retina. Increasing the proximity results in a larger area of activation because the stimulus amplitude needs to be increased to activate some body cells, thereby expanding the size of the phosphene. The shape of the phosphene is related to the spreading direction of current density from the active electrodes to ground. As the proximity increases with an increase of the stimulus amplitude, the current spread varies according to the topology of the electrode array and the position of the active and ground electrode. This will lead to changes in the area of stimulation, thereby causing the generation of phosphenes with shapes other than a small spot of light.

**Activation of Ganglion Cells:** There is a close association between the broadness of the activation area and the amount of peak current injected to the electrode, see percept breadth among charge densities in figure 6. That is, far-localized ganglion cells can be activated by increasing the injected current or charge. Experimental findings by Rizzo [25] in human volunteers demonstrated conclusively a direct relationship between the stimulus charge and the size of the percept.

Likewise, electrode topology plays a major role in the amount of body cells activated. A far placement of the ground to the active electrode causes a deep flow of the current into the tissue environment leading to the activation of cells in the interim to the ground.

Decreasing electrode dimensions generate higher resolution patterns of prosthetic-elicited activity that are closer to light-elicited patterns [41]. The prosthetic devices developed by Mahadevappa et al., [10], Rizzo et al., [12], Klauke et al., [13] Eger et al., [14] and Humayun et al., [16] used big-sized electrode diametersof 500, 200 and 100 μm, respectively. The electric current field from large electrodes indiscriminately drives local retinal activity in an abnormal way, leading to complex retinal responses [29].

**Drawbacks of the Activation Area:** The flexibility to trigger near or far localized cells should not be misinterpreted. Despite that a larger activation area influences a distant cell to be activated, the stimulus could reach undesirable localities where additional cells could be stimulated, thereby reducing focal activation and greatly decreasing resolution.

Safeguarding the operation of stimulators is a crucial issue in neural activation. Safety, in terms of electrical performance, is mainly related to three factors: charge density injection level, heat generated at tissue due to the power dissipation by the device, and the water-voltage window. Reducing electrode dimensions will generate small activation areas that could stimulate a single cell. However, thiscould cause a breakdown of the electrode and adverse tissue reactions due to a high charge density demand [41]. It is a general principle that the onset of irreversible Faradaic

Villarreal DL, Schroeder D, Krautschneider WH. A Treatise of the Physical Aspects of Phosphenes and Single-Cell Selectivity in Retinal Stimulation. *Int J Comput Neural Eng.* 2017;4(2):55-70.

63

processes should be avoided when body cells are activated. As a rule-of-thumb, the injected charge should be kept at low levels where it may be accommodated strictly by reversible charge injection processes. Electronics of any kind dissipates a certain amount of power. Temperature increase at tissue exhibits a linear relationship with power dissipation of $\Delta T = 1°C$ per $12.2mW/cm^2$ [42] assuming only heat conduction. Thus, as a rule-of-thumb, the implanted device should not exceed $12.2mW/cm^2$ of power.

## Single Cell Stimulation

A comparison is made between the electrode arrangement developed by Keserü and our proposal in terms of the broadness of the activation area and the number of activation of cells for the purpose of single cell stimulation. To make a fair comparison, a replica of the simulation model formerly explained is used, see figure 3.

**Methods.**

*Proposed Electrode Arrangement:* We proposed an evenly distributed 32 by 32 electrode array; see figure 7(a). The length, $l$, and width, $w$, of the electrode carrier are assumed to be equal and calculated as:

$$w = l = d \cdot \left( \sqrt{e_T} + 1 \right) \quad \text{---- (7)}$$

$e_T$ is the total number of electrodes inside the carrier. Let us call a square area-element inside the electrode carrier with sizes labeled as $d$, see figure 7(a), where $d$ is the electrode pitch.

$$d = \frac{1}{\sqrt{\rho_E}} \quad \text{---- (8)}$$

$\varrho_E$ is the electrode density. For given electrode diameter, the electrode distance can be computed as:

$$I_{ED} = d - E_D \quad \text{-----(9)}$$

$E_D$ is the electrode diameter and $I_{ED}$ represents the electrode distance. The electrode carrier area is:

$$A = l^2 \quad \text{----(10)}$$

*Procedure for Single-cell Selectivity:* Single-cell selectivity is treated as enhancing the control of the electrodes over single cells to produce an array of independent phosphenes [48]. Thus, the stimulus that spreads through the medium must be constrained to the space required for activation. To be precise, the discrimination of the area of stimulation must be generated such that the detail perception of the visual field of view is improved.

Nevertheless, a large proportion of ganglion cells are found in the central region within $\pm 10°$ of eccentricity away from the fovea. This region is needed for critical functions, such as object recognition, reading and driving [56]. With high density, ganglion cells may overlap with each other and may cause electrodes to activate more than a single cell.

To acquire a clear understanding of how electrodes activate some ganglion cells for the purpose of single-cell selectivity, we shall consider first the activation of cells in a perspective three-dimensional region; second a realistic distribution of RGC along the vertical section of the ganglionic layer and third a mathematical approach that ensures the activation of a single cell per stimulating electrode. The latter challenge shall provide the dimensions of the electrode carrier for realistic applications.

**Volume Region of Stimulation:** Consider an electrode array distributed equally with electrodes having a diameter and a density. The procedure to generate the volume region of stimulation consists in following the second path of the algorithm shown in figure 2.

The cell is shifted around the horizontal direction ($x$ or $y$ axis) and located at a distance of $d/2$ away from the active electrode, see figure 7(a). The algorithm is executed until the threshold injected current across the electrodes is found. Then, the cell is shifted around the horizontal and vertical direction ($z$ axis) to mark the places of stimulation using this threshold current. This will eventually lead to the volume region of stimulation.

Comsol produced a region of stimulation that consists of an area of activation bounded by the electrode pitches and a peak height $h$, all forming the volume of stimulation. The peak height of the volume region depends on the electrode diameter and density. Figure 7(b) illustrates the volume region of stimulation with the peak height, electrode pitches, and horizontal and vertical directions.

The area of activation is illustrated as a red dash-line boundary that follows a 'sinking at the diagonals' shape with an average distance of 80% of $d/2$. For simplicity, the activation area of each electrode is represented as a circular shape with a distance $d/2$ away from the active electrode. The area can be computed as $\pi d^2/4$.

**Realistic Distribution of Retinal Ganglion Cells:** Photomicrographs of the retina of healthy human [57, 58], monkey [59] and mice [60] were considered in the estimation of the RGC distribution along the vertical section.

In brief, we divided the ganglionic layer in horizontal segments of equal thickness and cell nuclei were counted for each segment. Then, the results were averaged, normalized and plotted in red with circular markers against the thickness of the ganglionic layer, see figure 7(c). It is also shown the normalized results of each reference in black using four different line styles.

The curve shape of the averaged and normalized data was fitted to a 3rd order polynomial. The curve peak amplitude was build such that the integral of the polynomial over the RGC thickness yields the same realistic amount of cells per $mm^2$ measured by Curcio et al., [61]. Thus, the polynomial $Az^3 + Bz^2 + Cz + D$ describes the volumetric cell density with numerical values of $D = 0$, $C = 3.7392 \, \rho_C/t^2$, $B = 0.741 \, \rho_C/t^3$, $A = -4.4802 \, \rho_C/t^4$, where t is the RGC thickness. As a reminder $\rho_C$ is the area cell density.

Here we assumed that the cell distribution along the vertical section behaves the same for all four meridians.

**Mathematical Approach for Single-cell Selectivity:** Consider an arbitrary electrode density and cell distribution. The approximation to activate a single cell per stimulating electrode

can be computed as:

$$\iiint_V \rho_V(z)\, dx\, dy\, dz = 1 \qquad \text{----- (11)}$$

$\rho_p$ is volumetric cell density described by the polynomial. $V$ is the volume region of stimulation. Let us assume that the shape of the volume of stimulation forms one half of a spheroid with two equal semi-diameters described as $d/2$. Using the relationship of $d^2 = 1/\rho_E$ and rearranging eq. (11) we get

$$\frac{\pi}{4\rho_E}\int_0^h \left(1 - \frac{z^2}{h^2}\right)\rho_V(z)\, dz = 1 \qquad \text{----- (12)}$$

where the peak height for an electrode diameter of 5 μm is fitted to $h(\rho_E, E_D) = \alpha \cdot \rho_E^{\beta}$ in millimeters with values of 0.087 for α and -0.2 for β. The implicit solution of eq. (12) yields

$$\frac{\pi}{2}\left(\frac{A}{24}\alpha^4 \rho_E^{-1.8} + \frac{B}{15}\alpha^3 \rho_E^{-1.6} + \frac{C}{8}\alpha^2 \rho_E^{-1.4}\right) - 1 = 0 \qquad \text{----(13)}$$

where Matlab is used to solve the roots of eq. (13). Since Matlab returned more than one solution, electrode pitches and peak heights of the volume of stimulation were determined using each electrode density, except of such with an imaginary part. Later, the volumes tested their stimulation of cells. The electrode density with cell activation closest to one is selected.

**Stimulation Parameters:** In this study, we set a boundary between 4° (1 mm) where peak cell density is located [61] and 10° (2.7 mm) [56] of eccentricities that covers critical functions such as object recognition, reading and driving and thus relevant for high resolution vision. Within this boundary, we tested the eccentricities of 1, 1.5, 2 and 2.7 mm.

Curcio [61] and Raza [62] measured in these eccentricities the area cell densities and RGC layer thicknesses for six retinas and 43 eyes of 36 human healthy controls, respectively. The results of each meridian are shown in table 2.

Throughout the study, single electrode stimulation is implemented

with electrode diameter of 5 μm. The stimulation arrangement consists of an active electrode (blue) surrounded by eight grounds (black), see fig. 7(a). The proximity of cells to the electrodes in fig. 7(b) is 10 μm.

Charge-imbalanced rectangular pulse shape was applied with anodic first phase of 100μs pulse duration followed by the cathodic phase of 50μs pulse duration. Between the anodic and cathodic phases, the system is open-circuited with a delay of 100 μs. The control of selecting the role of electrodes to function as active or ground is considered as seen in previous publications [31, 45]. Active electrodes can have their own time slot for stimulation [45].

Assembling the electrodes evenly gives the advantage for each active electrode to have eight surrounding grounds. The distribution of current density can be restricted in a small region that surrounds the ganglion cell. This results in a more controlled stimulation area [31].

### Results.

Figure 7(a) depicts the square area-element inside the electrode carrier with electrode pitches labeled as $d$. The cell is located at a distance $d/2$ away from the active electrode. A 32 by 32 electrode array was implemented in this study.

Figure 7(b) also shows the 3-dimensional stimulating region with the peak height, $h$, electrode pitches, activation areas represented as a gray dash-line, and horizontal and vertical directions. Figure 7(c) depicts a sketch of the retina along the vertical section. Cell nuclei counting results are shown inside the ganglionic layer.

Figure 7(d) shows the comparison of the electrode array developed by Keserü and our proposal in terms of the broadness of the activation area. Here, the maximum and minimum electrode pitches of 18.66 and 22.59μm with peak heights of 17.69 and 19.1 μm (electrode densities of 2871 and 1959 mm$^{-2}$) were simulated, producing almost the same amount of charge density of 0.1mC/cm² to obtain the activation area shown in fig. 7(b). Hence, the outcome of Keserü of single site electrode using the same charge density at proximity of 10 μm is compared, see figures. 6.7. All results throughout our simulations were within the

**Table 2. Cell Densities [mm$^{-2}$]/RGC Thicknesses [μm] From References.**

| Meridian/Eccentricity | 1 mm | 1.5 mm | 2 mm | 2.7 mm |
|---|---|---|---|---|
| Temporal | 26922/46 | 22897/47.5 | 16311/40 | 9642/28 |
| Nasal | 31544/56 | 27491/58.5 | 17037/46 | 8266/28.5 |
| Superior | 27118/60 | 18463/45 | 11622/35 | 6836/26 |
| Inferior | 26503/60 | 18007/45 | 9746/31 | 5412/25 |

**Table 3. Electrode Densities For Single-Cell Stimulation [mm$^{-2}$].**

| Meridian/Eccentricity | 1 mm | 1.5 mm | 2 mm | 2.7 mm |
|---|---|---|---|---|
| Temporal | 2871 | 2443 | 2421 | 2640 |
| Nasal | 2446 | 2084 | 2062 | 2300 |
| Superior | 1991 | 2253 | 2264 | 2238 |
| Inferior | 1959 | 2212 | 2334 | 1964 |

**Figure 7. (a)** Proposed electrode arrangement simulated in Comsol Multiphysics. Electrode pitch is labeled as *d*. Active and ground electrodes are highlighted in blue and black, respectively. A 32 x 32 electrode array was implemented. Electrodes have a diameter of 5μm. Width, *w*, and length, *l*, of the carrier are assumed to be equal. The electrodes are in contact with the retinal surface layer with proximity of 10 μm. **7(b)** A perspective three-dimensional view showing the stimulating region with peak height, *h*, electrode pitches, proximity of cells to the electrodes and horizontal and vertical directions. Comsol gave the activation area shown a as red dash-line that follows a 'sinking at the diagonals' shape with an average distance of 80% of *d*/2. For simplicity the activation area is represented as a circular shape with some distance *d*/2 away from the electrode. Thus, the activation areas are represented as a gray dash-line and are observed to have a form such that the overlapping with adjacent activation areas is avoided. **Figure 7(c)** shows a sketch of the retina along the vertical section. Cell nuclei counting results are shown inside the ganglionic layer. Thickness of each layer is not drawn to scale. **7(d)** Comparison of the broadness of the activation area between the electrode arrangement developed by Keserü and our proposal. Here, the maximum and minimum electrode pitches of 18.66 and 22.59 μm with peak heights of 17.69 and 19.1 μm (electrode densities of 2871 and 1959 mm$^{-2}$) were simulated, yielding roughly a charge density of 0.1 mC/cm$^2$ to obtain the activation area shown in figure. 7(b). Thus, the result of Keserü of single site electrode using the same charge density at proximity of 10 μm was compared, see figure. 6.7. **7(e)** depicts the mean and deviation of stimulation, y-axis, against electrode densities, x-axis. The red line crossing the plot at a value of one indicates single cell activation.
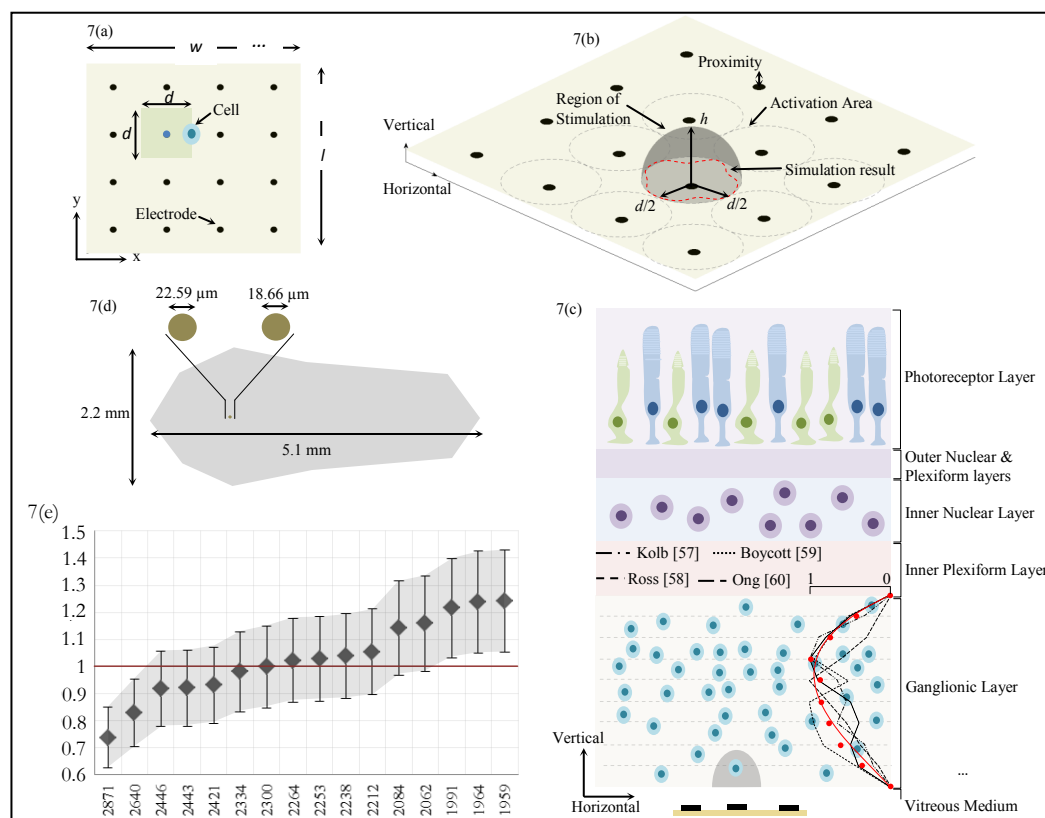


electrochemical safety region.

Eq. (13) was solved for the electrode density using the data provided by Curcio and Raza of area cell densities and RGC layer thicknesses (table 2). As such, the electrode density can provide parameters for the electrode carrier that allow the activation of a single cell per stimulating electrode. Table 3 lists the results.

Since electrode density cannot be altered after implantation, we sought for a single value of electrode density for realistic applications. Thus, electrode pitches and peak heights of the volume of stimulation were determined using the data of table 3. Then the volumes tested their activation of cells for every distribution described by the polynomial using the data of Table 2. The mean and standard deviation of stimulation were determined for each electrode density. These results are shown in Figure 7(e), y-axis, against electrode densities, x-axis. The winner is based on a mean having a minimal distance from one (indicating single cell

selectivity) and preferably small deviation of the mean.

**Discussion.**

In this study, we reached the stimulation of a single cell per stimulating electrode and small activation areas throughout the boundary of eccentricities relevant for high resolution vision. The results included cell densities from 31544 to 5412 mm$^{-2}$. This leads to electrode densities between 2446 and 1964 mm$^{-2}$, electrode pitches between 20.21 and 22.56μm and an activation area per stimulating electrode from 320 to 399 μm$^2$. The visual angles (horizontal or vertical) reached 0.068° and 0.076° per electrode site, all respectively, meaning a more precise stimulation region.

As previously stated, Keserü generated stimulation areas from 1.6 to 44.88 mm$^2$ and from 4.03 to 121.04 mm$^2$ for single and multiple electrode stimulation, all respectively, see Figure 6. The vertical and horizontal visual angles are from 4.3 and 4.8° to 18.5

Villarreal DL, Schroeder D, Krautschneider WH. A Treatise of the Physical Aspects of Phosphenes and Single-Cell Selectivity in Retinal Stimulation. *Int J Comput Neural Eng*. 2017;4(2):55-70.

and 36° for single electrode stimulation. For multiple electrode stimulation the visual angles are from 6.7 and 9° to 35 and 50.2°, all respectively. These large oblong-like shapes of light lessen the quality of vision and cause image sharpness and detail perception to be reduced.

Shown in Figure 7(b), the activation area for each electrode is observed to have a form such that the overlapping with adjacent activation areas is circumvented. This can be achieved firstly by having a different time slot of stimulation and secondly by controlling the electrodes to play a role of being either active or ground. This provides the benefit that the spreading of current density can be confined in a small region that surrounds the cell. This results in a more controlled stimulation area. Figure 7(d) shows that our stimulation strategy produces a narrower activation area than either single or multiple electrode configurations used in Keserü M, et al., (2012) [15]. This activation area may enhance the detail perception of the visual field of view. This is due because the stimulus that spreads throughout the medium can be confined to the space required for activation. As such, the discrimination of the area of stimulation can be generated.

However, these results underline the necessity of using electrodes with dimensions lower than the electrode pitch for realistic applications. In general, an array of 32 by 32 electrodes with square-grid distribution, 10 μm of proximity or below and electrode size of 5 μm, all within the eccentricities tested, can deliver safe stimulus using charge-imbalanced rectangular pulse shape with anodic first phase of 100μs pulse duration followed by the cathodic phase of 50μs pulse duration. This is valid for limits of charge density of 1 mC/cm², neural tissue heating of 1°C, and electrode voltage of 1.7V.

In spite that reaching single cell selectivity can enhance visual perception [63], the electrodes need to be positioned close to each other in the carrier. This would lead to a more detailed stimulating region. However, this causes that the visual field of view generated by stimulation may be small because it is directly related to the size of the stimulated area at the retina and hence to the size of the electrode carrier. Using eq. (5) it is estimated that the projected visual field of view for every 1 mm of the retina is about 3.37°. Tychsen [64] estimated a similar value of 3.35°. Using the minimum and maximum electrode carrier area of 0.37 and 0.55 mm² (electrode densities of 2871 and 1959 mm⁻², respectively), the visual field of view would cover 2.04° by 2.04° for electrode carrier of 0.37mm² and 2.5° by 2.5° for 0.55 mm². Current visual devices can provide visual angles higher than 10° [16]. This is required to perform simple navigation tasks, recognize large objects and distinguish the direction of movement [65]. Despite that those cannot generate single-cell activation per electrode which would produce independent pixels, there is hope to achieve such challenges. Meza et al., [45] suggested the use of daisy chain configuration to connect the required amount of chips with hybrid architecture current steering that enables low power consumption and high channel integration on a small chip area. This method can increase the number of stimulation channels and generate a large area of stimulationat the retina while preserving detail perception.

The array developed by Keserü, as opposed to our approach that reached a single cell per stimulating electrode, used large electrodes that activate between 30912 and 124776 for single-site

and between 37492 and 340028 for multiple-site, see Figure 6, respectively, assuming to place the electrode array as shown in Figure 4(d). This coarse activation of cells not only constrains the detail perception, but also the activity generated by stimulation remains different from a healthy retina.

Lastly, figure 7(e) shows the mean and standard deviation of stimulation against the electrode densities. As we sought for a single value for realistic applications, electrode density of 2300 is suitable for placement within ±10° of eccentricity by having a mean with minimal distance from one (indicating single cell activation) and having a small deviation as previously stated.

## Supporting Evidence

There are mainly five numerically dominant retinal ganglion cell classes: ON and OFF midget, ON and OFF parasol, and small bistratified. Midget cells constitute the most densely visual pathway in the primate retina with a percentage of about 80% [66]. Parasol [67] and bistratified [66] cell classes represent about 20% of all ganglion cells.

Despite that ON and OFF type ganglion cells exhibit different light-response properties [68], retinal connectivity [69] and dendritic tree breadth [70], the activation threshold for these two cell types is not statistically different both for epiretinal [71] and subretinal [72] stimulation. Experimental findings by Jepson [73] indicated similar thresholds for electrical stimulation of the five numerically dominant retinal ganglion cell types previously mentioned. These findings indicate that ON and OFF type cells fire temporally in phase [74]. ON and OFF type cells can be stimulated with arrays of electrodes with small diameter at comparable threshold levels [71]. Margalit [75] reported similar findings in tiger salamander retina. In many cases, a single cell could be individually stimulated without activating adjacent cells of the same type or other types [73].

Before hand that any stimulation is given, patients report a grayish background covering their visual fields [76]. In response to direct activation of ganglion cells with electric stimulus, patients frequently report a bright percept that is surrounded by a dark background [7, 25, 77]. The brightness or darkness of the elicited phosphene may be involved as to whether the ON or OFF pathways are being stimulated. Freeman et al., [74] suggested the possibility that the OFF pathway is outweighed by the signal from the ON pathway when both are activated identically by electric stimulation. Another possibility is that a bright phosphene results from preferential activation of ON versus OFF type ganglion cells.

While the electrodes stimulate nearby RGCs, the phosphene frequently reported by the patients can be related to the response of a cluster of ON type cells, see Figure 8. This is because ON and OFF type cells are spatially intermixed [78] and the bright response of ON type cells overshadows the response of OFF cells and their activation is more preferred [74]. While the stimulus is delivered to the cells, the activation area can indicate the stimulation of RGCs regardless of the type and class because they have similar activation thresholds [71-73]. ON and OFF type cells are contained within the activation area. Thus, the activation area can estimate the amount of RGCs stimulated with a given set of stimulation parameters.

Villarreal DL, Schroeder D, Krautschneider WH. A Treatise of the Physical Aspects of Phosphenes and Single-Cell Selectivity in Retinal Stimulation. *Int J Comput Neural Eng.* 2017;4(2):55-70.

67

**Figure 8. Relation between the phosphene elicited by electrical stimulus and the activation area. The phosphene frequently reported by the patients can be related to the response of a cluster of ON type cells. The activation area shown with white outline can estimate the size and shapes of the elicited phosphene because it indirectly shows an area that can be related to the bright response of ON type cells.**
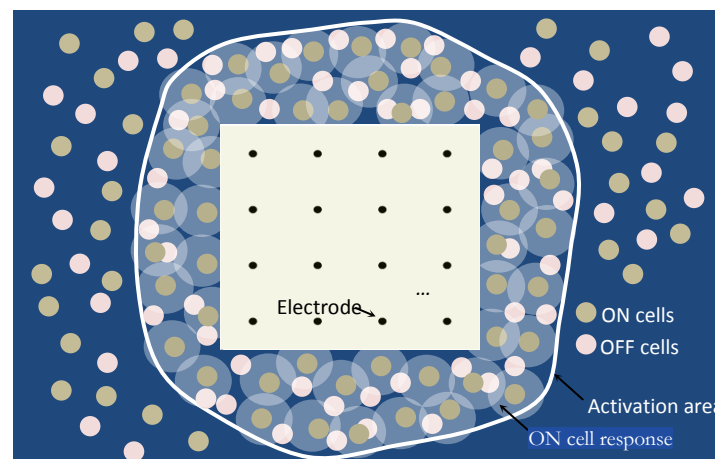


Regarding the estimation of the size and shape of the phosphene while the activation area is used: despite that the activation area indicates the stimulation of RGCs regardless of the type and class, the activation area can estimate the physical aspects of the elicited phosphene because it implicitly shows an area that can be related to the bright response of ON type cells., see Figure 8. This indirect approach to map the elicited phosphene relates to the respond of actual ON type cells being electrically stimulated.

However the area of activation can have discrepancies with the actual elicited phosphene when the degree of retinal degeneration of ON type cells is high. This can influence the shape of the visual perception because gaps of dark vicinities would be exhibited at locations of cell depletion.

That being said, we found that the shape and size of the phosphenes are directly influenced by the electrode topology, characteristics of the electrodes, cell density at the degenerate retina, stimulating electrode configuration, closeness of the electrodes to the cells and the peak amplitude of the stimulus.

Intrinsically, the strategy of the activation area is linked to the common goals of stimulating a single ganglion cell and producing a small spot of light required for high-resolution. It can yield key advantages to design optimal electrode arrays and optimal stimulus parameters for artificial vision.

**Limitations**

A key challenge of artificial visual devices is to avoid the stimulation of retinal ganglion cell axons [48].

Retinal ganglion cell axons pass within short distances from each other along their path to the brain. Since images are reversed horizontally and vertically on the retina by the optics of the cornea and lens, stimulation on the left side of the retina should create perceptions in the right side and vice versa. If the retinal axons coming from cells in the periphery are as well stimulated, then the perception would reflect activation of those peripheral cells and appear as an ellipse or streak [48]. In practice, though,

while subjects receive single electrode stimulus, they often report a stripe-shaped phosphene, rather than a focal spot of light. This may be caused by unintended stimulation of passing axons [54].

This issue has been addressed by Jensen and Rizzo III [79]. In their study, short-current pulses of 100μs or less are preferable because passing retinal ganglion cell axons can be avoided while stimulation. Choosing that pulse duration, the amount of current needed to generate the response of a cell is much lower than that required to generate an axonal response. Greenberg et al., supported these observations by reporting that axonal threshold was 20% higher than that of the retinal ganglion cell [80]. Experimental findings by Jepson [63] exhibited single spike responses with sub-millisecond latency which is a characteristic of direct ganglion cell activation. In this study, short pulse durations of 100 μs and small electrodes of 15 μm of diameter were used.

The ratio of axonal to cell threshold current recorded by Jensen and Rizzo III was 4 for electrode diameter of 125 μm. These results are related to use the threshold or minimum current to activate retinal ganglion axons and cells. Short-current pulses have an additional advantage of reducing the charge required for excitation. With reduced charge, the probability of electrode corrosion and tissue damage is lessened [79].

Regarding our simulation-based findings, the minimum threshold to activate a cell was increased to stimulate a cell at a distance $d/2$ away from the active electrode. This approach may increase the concern of generating an axonal response. The ratio of the maximum to the minimum injected current in our study is 2.5, which is less than the ratio found by Jensen and Rizzo III. However, further experimental tests are required to validate our results. Through our study, short-current pulse of 100 μs was used.

**Conclusion**

An accurate explanation of the activation area and its benefits to achieve single-cell selectivity are presented in this report. The reasoning of how phosphenes are generated by electrical stimulation can be better understood by applying in practice

Villarreal DL, Schroeder D, Krautschneider WH. A Treatise of the Physical Aspects of Phosphenes and Single-Cell Selectivity in Retinal Stimulation. *Int J Comput Neural Eng.* 2017;4(2):55-70.

68

the activation area. We found that the shape and size of the phosphenes are directly influenced by the electrode topology, characteristics of the electrodes, cell density at the degenerate retina, stimulating electrode configuration, the closeness of the electrodes to the cells and the peak amplitude of the stimulus. The activation area is linked to the common goals of stimulating a single ganglion cell and producing a small spot of light required for high-resolution vision.

Thus, prior to device implantation at the retina, simulation-based findings of the activation area can be beneficial to understand life like situations of phosphenes. The robustness of our technique is such that any cell density can be evaluated to direct visual prosthetic devices towards single localized stimulation. This would result to a more precise region of stimulation and to a high-resolution vision.

## Acknowledgment

## References

[1]. Spencer C Chen, Gregg J Suaning, John W Morley, Nigel H Lovell. Simulating prosthetic vision: I. Visual models of phosphenes. Vision Res. 2009 Jun;49(12):1493–1506.

[2]. Križaj D, Ryskamp DA, Tian N, Tezel g, Mitchell CH, Slepak VZ, et al. From mechanosensitivity to inflammatory responses: new players in the pathology of glaucoma. Curr Eye Res. 2014 Feb;39(2):105–119.

[3]. Bonmassar G, Seung Woo Lee, Daniel K Freeman, Miloslav Polasek, Shelley I Frie, John T Gale. Microscopic magnetic stimulation of neural tissue. Nat Commun. 2012 Jun 26;3:921.

[4]. Walsh G, Barlow H, Kohn HI. Magnetic stimulation of the human retina. Fed Proc. 1946;5(1 pt 2):109–110.

[5]. Walsh V, Cowey A. Magnetic stimulation studies of visual cognition. Trends Cogn Sci. 1998 Mar 1;2(3):103–110.

[6]. Humayun MS, E de Juan, G Dagnelie, RJ Greenberg, RH Probst, DH Phillips. Visual perception elicited by electrical stimulation of retina in blind humans. Archive of Ophthalmol. 1996 Jan;114(1):40-46.

[7]. Humayun MS, E de Juan, JD Weiland, G Dagnelie, S Katona, R Greenberg, et al. Pattern electrical stimulation of the human retina. Vision Res. 1999 Jul;39(15):2569–2576.

[8]. Humayun MS, JD Weiland, GY Fujii, R Greenberg, R Williamson, J Little, et al. Visual perception in a blind subject with a chronic microelectrode retinal prosthesis. Vision Res. 2003 Nov;43(24): 2573–2581.

[9]. Humayun MS, Yanai D, Greenberg RJ, Little J, Mech BV, Mahadevappa M, et al. Clinical results with the model 1IRP implant. Neural networks, Proceedings. 2004 IEEE International Joint Conference on 2004 Jul 25-29; IEEE: Budapest, Hungary. 2005 Jan 17.

[10]. Mahadevappa M, Weiland J, Yani D, Fine I, Greenberg R, Humayun, M. Perceptual thresholds and electrical impedance in 3 retinal prosthesis subjects. IEEE Transactions on Neural System Rehabilitation Engineering. 2005 Jun 13;13(2):201-206.

[11]. Rizzo JF, JL Wyatt. Review: Prospects for a visual prosthesis. Neuroscientist. 1997 Jul 1;3(4):251-262.

[12]. Rizzo JF, JL Wyatt, Loewenstein J, Kelly S, Shire D. Methods and Perceptual Thresholds for Short-Term Electrical Stimulation of Human Retina with Microelectrode Arrays. Investigative Ophthalmol Vis Sci. 2003 Dec;44(12):5355-61.

[13]. Klauke S, Goertz M, Rein S, Hoehl D, Thomas U, Eckhorn R, et al. Stimulation with a Wireless Intraocular Epiretinal Implant Elicits Visual Percepts in Blind Humans. Invest Ophthalmol Vis Sci. 2011 Jan 21;52(1):449-455. doi:10.1167/iovs.09-4410.

[14]. Eger M, Reinhard Eckhorn, Marcus Wilms, Thomas Schanze. Visual resolution with retinal implants estimated from recordings in cat visual cortex. Vision Res. 2006 Sep;46(17):2675–2690.

[15]. Keserü M, Feucht M, Bornfeld N, Laube T, Walter P, Hornig R, et al. Acute electrical stimulation of the human retina with an epiretinal electrode array. Acta Ophthalmol. 2012 Feb;90(1):e1-8. Epub 2011 Nov 8.

[16]. Humayun M, Dorn DJ, da Cruz L, Sahel JA, Eliott D, Ho AC, et al. Interim results from the international trial of second sight's visual prosthesis. Ophthalmology. 2012 Apr;119(4):779–788.

[17]. Stingl K, Besch D, Braun A, Hipp S, Schatz A, Peters T, et al. Artificial vision with wirelessly powered subretinal electronic implant alpha-IMS. Proc Biol Sci. 2013 Feb 20;280(175):20130077.

[18]. Dobelle WH, Mladejovsky MG, Girvin JP. Artificial vision for the blind: Electrical stimulation of visual cortex offers hope for a functional prosthesis. Sci. 1974 Feb 1;183(4123):440-444.

[19]. Dobelle WH. Artificial vision for the blind by connecting a television camera to the visual cortex. ASAIO J. 2000 Feb;46(1):3–9.

[20]. Zrenner E, Besch D, Bartz-Schmidt KU, Gekeler F, Gabel VP, Kuttenkeuler C, et al. Subretinal chronic multi-electrode arrays implanted in blind patients. IOVS. 2006 May;47(13):1538.

[21]. Zrenner E, Wilke R, Zabel T, Sachs H, Bartz-Schmidt K, Gekeler F, et al. Psychometric analysis of visual sensations mediated by subretinal microelectrode arrays implanted into blind retinitis pigmentosa patients. IOVS. 2007 May;48:659.

[22]. Brindley GS, Lewin W. The sensations produced by electrical stimulation of the visual cortex. J Physiol. 1968 May;196(2):479-493.

[23]. Brindley GS, Rushton DN. Properties of cortical electrical phosphenes. In: SJ Cool, EJ Smith, editors. Frontiers in visual science. New York: Springer-Verlag;1978.

[24]. Hornig R, Laube T, Walter P, Rossler G, Wyatt J, Richard G, et al. A method and technical equipment for an acute human trial to evaluate retinal implant technology. J Neural Eng. 2005 Mar;2(1):S129–S134.

[25]. Rizzo JF, Wyatt J, Loewenstein J, Kell S, Shire D. Perceptual efficacy of electrical stimulation of human retina with a microelectrode array during short-term surgical trials. Invest Ophthalmol Vis Sci. 2003 Dec;4(12):5362–5369.

[26]. Veraart C, Raftopoulos C, Mortimer JT, Delbeke J, Pins D, Michaux, G, et al. Visual sensations produced by optic nerve stimulation using an implanted self-sizing spiral cuff electrode. Brain Res. 1998 Nov;813(1):181–186.

[27]. Weiland JD, Yanai D, Mahadevappa M, Williamson R, Mech BV, Fujii GY, et al. Electrical stimulation of retina in blind humans. proceedings of the 25th annual international conference of the IEEE, engineering in medicine and biology society. 2003 Sep 17-21. IEEE: Cancun, Mexico; 2004 Apr 5.

[28]. LH Jepson, Hottowy P, Gunning DE, Litke AM, Dabrowski W, Chichilnisky EJ, et al. Spatially Patterned Electrical Stimulation to Enhance Resolution of Retinal Prostheses. J Neurosci. 2014 Apr 2;34(14):4871– 4881.

[29]. Horsager A, Fine I. The perceptual effects of chronic retinal stimulation. In: G Dagnelie, editor. Visual Prosthetics: Physiology, Bioengineering, Rehabilitation. Springer US; 2011. 271-300. DOI: 10.1007/978-1-4419-0754-7_14.

[30]. Weitz AC, Nanduri D, Behrend MR, Greenberg RJ, Chow RH, et al. Improving the spatial resolution of epiretinal implants by increasing stimulus pulse duration. Sci Transl Med. 2015 Dec 16;7(318):318ra203.

[31]. Luján Villarreal D, Dietmar Schroeder, Wolfgang H Krautschneider. Feasibility Study of a 1000+ Electrode Array in Epiretinal Prosthesis. Intl J Pharma Med Bio Sci. 2016 Jul;5(3):163-170. 10.18178/ ijpmbs.5.3.163-170.

[32]. Starbird R. Study of organic materials to improve electrical properties of neural stimulation electrodes. Dissertation, 2013.

[33]. Kasi H, W Hasenkamp, G Cosendai, A Bertsch, P Renaud. "Simulation of epiretinal prostheses - Evaluation of geometrical factors affecting stimulation thresholds. J Neuroeng Rehabil. 2011 Aug 19;8:44.

[34]. Werginz P, H Benav, E Zrenner, F Rattay. Modeling the response of ON and OFF retinal bipolar cells during electric stimulation. Vision Res. 2015 Jun;111(Pt B):170-181. Epub 2014 Dec 11.

[35]. Abramian M, NH Lovell, JW Morley, GJ Suaning, S Dokos, Computational model of electrical stimulation of a retinal ganglion cell with hexagonally arranged electrodes. Conf Proc IEEE Eng Med Biol Soc. 2012;2012:3029-32.

[36]. Yin S, NH Lovell, GJ Suaning, S Dokos. A continuum model of the retinal network and its response to electrical stimulation. Conf Proc IEEE Eng Med Biol Soc. 2010;2010:2077-80.

[37]. Kameneva T, H Meffin, AN Burkitt. Modelling intrinsic electro physiological properties of ON and OFF retinal ganglion cells. J. Comput Neurosci. 2011;31(3):547-61.

[38]. Fohlmeister J, PA Coleman, RF Miller. Modeling the repetitive firing of retinal ganglion cells. Brain Res. 1990 Mar 5;510(2):343-345.

[39]. Hodgkin A, Huxley AF. A quantitative description of membrane current and its application to conduction and excitation in nerve. J Physiol. 1952 Aug 28;117(4):500-544.

Villarreal DL, Schroeder D, Krautschneider WH. A Treatise of the Physical Aspects of Phosphenes and Single-Cell Selectivity in Retinal Stimulation. *Int J Comput Neural Eng.* 2017;4(2):55-70.

69

[40]. Joucla S, Gliere A, Yvert B. Current approaches to model extracellular electrical neural microstimulation. Front Comput Neurosci. 2014 Feb 19;8:13. 8:13.

[41]. Fried S, Hsueh HA, Werblin FS. A Method for Generating Precise Temporal Patterns of Retinal Spiking Using Prosthetic Stimulation. J Neurophysiol. 2006 Feb;95(2):970–978.

[42]. Sohee K, Normann RA, Harrison R, Solzbacher F. Preliminary study of the thermal impact of a microelectrode array implanted in the brain. Conf Proc IEEE Eng Med Biol Soc. 2006;1:2986-9.

[43]. Duay J, Eleanor Gillette, Ran Liu, Sang Bok Lee. Highly flexible pseudocapacitor based on freestanding heterogeneous MnO2/conductive polymer nanowire arrays. Phys Chem Chem Phys. 2012 Mar 14;14(10):3329–3337.

[44]. Singh V, A Roy, R Castro, K McClure, R Dai, R Agrawal, et al. On the thermal elevation of a 60-electrode epiretinal prosthesis for the blind. IEEE transactions on biomedical circuits and systems. 2008 Nov 18; IEEE circuits and systems society IEEE engineering in medicine and biology society; 2008.

[45]. Meza-Cuevas M, D Schroeder, WH Krautschneider. A scalable 64 channel neurostimulator based on a hybrid architecture of current steering DAC. Biomedical engineering (MECBME), 2014 middle east conference; 2014 Feb 17-18; IEEE: Doha, Qatar; 2014 Apr 7.

[46]. Watson AB. A formula for human retinal ganglion cell receptive field density as a function of visual field location. J Vis. 2014 Jun 30;14(7):15.

[47]. Curcio C, Allen KA. Topography of Ganglion Cells in Human Retina. J Comp Neurol. 1990 Oct 1;300(1):5-25.

[48]. Weiland JD, Mark S Humayun. Retinal Prosthesis. IEEE transactions on biomedical engineering. 2014 May; IEEE engineering in medicine and biology society. 2014 Apr 2.

[49]. Meyer RD, Cogan SE, Nguyen TH, Rauh RD. Electrodeposited iridium oxide for neural stimulation and recording electrodes. IEEE Trans Neural Syst Rehabil Eng. 2001 Mar;9(1):2-11.

[50]. Weiland JD, Anderson DJ. Chronic neural stimulation with thin-film, iridium oxide electrodes. IEEE Trans Biomed Eng. 2000 jul;47(7): 911-918.

[51]. Niebauer MJ, Wilkoff B, Yamanouchi Y, Mazgalev T, Mowrey K, Tchou P. Iridium oxide–coated defibrillation electrode : reduced shock polarization and improved defibrillation efficacy. Circulation. 96(10):3732-3736.

[52]. Jan E, Hendricks JL, Husaini V, Richardson-Burns SM, Sereno A, Martin DC, et al. Layered carbon nanotube-polyelectrolyte electrodes outperform traditional neural interface materials. Nano Lett. 2009 Sep 28;9(12):4012-8.

[53]. Ware C. Information Visualization: Perception for Design. 2nd ed. Morgan Kaufmann; 2004 May 7.

[54]. Nanduri D, I Fine, A Horsager, GM Boynton, MS Humayun, RJ Greenberg, et al. Frequency and amplitude modulation have different effects on the percepts elicited by retinal stimulation. Invest Ophthalmol Vis Sci. 2012 Jan 20;53(1):205–214.

[55]. Wilke R, Gabel VP, Sachs H, Bartz Schmidt KU, Gekeler F, Besch D, et al. Spatial Resolution and Perception of Patterns Mediated by a Subretinal 16-Electrode Array in Patients Blinded by Hereditary Retinal Dystrophies. Invest Ophthalmol Vis Sci. 2011 July 29;52(8): 5995-6003. doi:10.1167/iovs.10-6946.

[56]. Nelson P, Aspinall P, Papasouliotis O, Worton B, O'Brien C. Quality of life in glaucoma and its relationship with visual function. J Glaucoma. 2003 Apr;12(2):139–150.

[57]. Kolb H, Fernandez E, Nelson R, editors. Webvision: The Organization of the Retina and Visual System [Internet]. Salt Lake City (UT): University of Utah Health Sciences Center; 1995.

[58]. Ross MH, Kaye GI, Pawlina W. Histology, a Text and Atlas. 4th ed. Philadelphia: Lippincott Williams & Wilkins; 2003.

[59]. Boycott B, Dowling J (1969) Organization of the primate retina: light microscopy. Phil Trans Roy Soc B. 1969 Mar 27;225:109-184.

[60]. Ong J, Zorapapel NC, Rich KA, Wagstaff RE, Lambert RW, Rosenberg SE, et al. Effects of Cholesterol and Apolipoprotein E on Retinal Abnormalities in ApoE-Deficient Mice. Invest Ophthalmol Vis Sci. 2001 July;42(8):1891-1900.

[61]. Curcio C, Allen KA. Topography of Ganglion Cells in Human Retina. J Comp Neurol. 1990 Oct 1;300(1):5-25.

[62]. Raza A, Hood C. Evaluation of the Structure–Function Relationship in Glaucoma Using a Novel Method for Estimating the Number of Retinal Ganglion Cells in the Human Retina. Invest Ophthalmol Vis Sci. 2015 Aug;56(9):5548–5556.

[63]. Jepson LH, Hottowy P, Mathieson K, Gunning DE, Dąbrowski W, Litke AM, et al. Spatially Patterned Electrical Stimulation to Enhance Resolution of Retinal Prostheses. J Neurosci. 2014 April 2;34(14):4871-4881.

[64]. Tychsen L. Binocular Vision. In: William M. Hart, editor. Adler's Physiology of The Eye. St. Louis: Mosby; 1992. 773–853.

[65]. Tombran-Tink J, Colin J Barnstable, Joseph F Rizzo. Visual Prosthesis and Ophthalmic Devices: New Hope in Sight. Newyork: Springer Science & Business Media; 2007 Dec 8.

[66]. Bigun J. Vision with Direction: A Systematic Introduction to Image Processing and Computer Vision. Newyork: Springer Science & Business Media; 2006 Feb 9.

[67]. Rodieck RW. The first steps in seeing. Sunderland: Sinauer; 1-485.

[68]. Chichilnisky EJ, Kalmar RS. Functional asymmetries in ON and OFF ganglion cells of primate retina. J Neurosci. 2002 Apr 1;22(7):2737–2747.

[69]. Sterling P, Demb JB. Retina. In: Shepherd GM, editor. The synaptic organization of the brain. 5th ed. New York: Oxford UP; 2004 Jan.

[70]. Peichl L, Ott H, Boycott BB. Alpha ganglion cells in mammalian retinae. Proc R Soc Lond B Biol Sci. 1987 Jul 22;231(1263):169–197.

[71]. Sekirnjak C, Hottowy P, Sher A, Dabrowski W, Litke AM, Chichilnisky EJ. High-resolution electrical stimulation of primate retina for epiretinal implant design. J Neurosci. 2008 Apr 23;28(17):4446–56.

[72]. Tsai D, Morley JW, Suaning GJ, Lovell NH. Direct activation and temporal response properties of rabbit retinal ganglion cells following subretinal stimulation J. Neurophysiol. 2009 Nov;102(5): 2982–93.

[73]. Jepson LH, Hottowy P, Gunning DE, Litke AM, Mathieson K, et al. Focal Electrical Stimulation of Major Ganglion Cell Types in the Primate Retina for the Design of Visual Prostheses. J Neurosci. 2013 Apr 24;33(17):7194–7205.

[74]. Freeman DK, Rizzo JF, Fried SI. Encoding visual information in retinal ganglion cells with prosthetic stimulation. J Neural Eng. 2011 Jun;8(3):035005.

[75]. Margalit E, Thoreson WB. Inner retinal mechanisms engaged by retinal electrical stimulation. Invest Ophthalmol Vis Sci. 2006 Jun;47(6):2606-2612.

[76]. Horsager A, Greenberg RJ, Fine I. Spatiotemporal interactions in retinal prostheses subjects. Invest Ophthalmol Vis Sci. 2010 Feb;51(2):1223–2333.

[77]. Zrenner E, Karl Ulrich Bartz-Schmidt, Heval Benav, Dorothea Besch, Anna Bruckmann, Veit-Peter, et al. Subretinal electronic chips allow blind patients to read letters and combine them into words. Proc Biol Sci. 2011 May 22;278(1711):1489–97.

[78]. Dacey DM. Origins of perception: retinal ganglion cell diversity and the creation of parallel visual pathways. In: Gazzaniga MS, editor. The cognitive neurosciences. Cambridge, MA: MIT; 2004. 281–301.

[79]. Jensen RJ, Ofer R Ziv, Joseph F Rizzo. Thresholds for Activation of Rabbit Retinal Ganglion Cells with Relatively Large, Extracellular Microelectrodes. Invest Ophthalmol Vis Sci. 2005 Apr;46(4):1486–1496.

[80]. Greenberg RJ, TJ Velte, MS Humayun, GN Scarlatis, E de Juan. A computational model of electrical stimulation of the retinal ganglion cell. IEEE Trans Biomed Eng. 1999 May;46(5):505-514.

Villarreal DL, Schroeder D, Krautschneider WH. A Treatise of the Physical Aspects of Phosphenes and Single-Cell Selectivity in Retinal Stimulation. *Int J Comput Neural Eng.* 2017;4(2):55-70.

70